Ab initio phonon dispersion in crystalline naphthalene using van der Waals density functionals

Florian Brown-Altvater,[1,2,*] Tonatiuh Rangel,[2,3] and Jeffrey B. Neaton[2,3,4,†]

[1]*Department of Chemistry, University of California, Berkeley, California 94720, USA*
[2]*Molecular Foundry, Lawrence Berkeley National Laboratory, Berkeley, California 94720, USA*
[3]*Department of Physics, University of California, Berkeley, California 94720, USA*
[4]*Kavli Energy NanoSciences Institute at Berkeley, Berkeley, California 94720, USA*

Acene molecular crystals are of current interest in organic optoelectronics, both as active materials and for exploring and understanding new phenomena. Phonon scattering can be an important facilitator and dissipation mechanism in charge separation and carrier transport processes. Here, we carry out density functional theory (DFT) calculations of the structure and the full phonon dispersion of crystalline naphthalene, a well-characterized acene crystal for which detailed neutron-diffraction measurements, as well as infrared and Raman spectroscopy, are available. We evaluate the performance, relative to experiments, of DFT within the local density approximation (LDA); the generalized gradient approximation of Perdew, Burke, and Ernzerhof (PBE); and a recent van der Waals–corrected nonlocal correlation (vdW-DF-cx) functional. We find that the vdW-DF-cx functional accurately predicts lattice parameters of naphthalene within 1%. Intermolecular and intramolecular phonon frequencies across the Brillouin zone are reproduced within 7.8% and 1%, respectively. As expected, LDA (PBE) underestimates (overestimates) the lattice parameters and overestimates (underestimates) phonon frequencies, demonstrating their shortcomings for predictive calculations of weakly bound materials. If the unit cell is fixed to the experimental lattice parameters, PBE is shown to lead to improved phonon frequencies. Our study provides a detailed understanding of the phonon spectrum of naphthalene, and highlights the importance of including van der Waals dispersion interactions in predictive calculations of lattice parameters and phonon frequencies of molecular crystals and related organic materials.

I. INTRODUCTION

Organic optoelectronic materials have attracted significant recent attention due to their relatively low production cost, abundance, simple processing techniques, and compatibility with flexible technologies, such as printed electronics [1,2] or wearable photovoltaics [3]. In particular, organic materials based on small molecules have shown great promise for optoelectronic applications, exhibiting high electron mobilities [4–8] and novel excited-state phenomena such as singlet fission [9–14]. However, despite significant promise, understanding and control of the mechanisms underlying these phenomena in organic crystals is still lacking [8,15]. As those processes are often subject to scattering from phonons, for example, leading to phonon-assisted transport and dissipation [8,16], a detailed, quantitative understanding of the vibrational spectra—and in particular, the phonon spectra of extended molecular crystals—is integral to future efforts to better harness these materials for optoelectronic applications.

Prior *ab initio* studies of organic crystals, based on density functional theory (DFT) and many-body perturbation theory, have focused predominantly on electronic and optical properties [17–28]. Such excited-state properties are sensitive to local geometry and molecular packing, and a principal challenge to theory is that long-range dispersive van der Waals (vdW)-type interactions play a significantly larger role for the cohesive energies (and therefore the geometries) of sparse molecular

crystals compared to their inorganic counterparts [22,29,30]. To account for vdW interactions quantitatively, several new functionals and a-posteriori corrections to DFT have been developed and are continuously being improved. Notable examples are the vdW nonlocal functionals of the vdW-DF family [31–33], and pairwise approaches such as those of Tkatchenko and Scheffler (and its many-body extensions) [34–37], Grimme [38–40], and Silvestrelli [41,42].

Among molecular crystals, the acene family is well suited for detailed study of vibrational and optoelectronic phenomena. Their relatively simple molecular and crystal structures—and variable size range, from benzene to hexacene—have facilitated significant experimental as well as computational investigation. Naphthalene is the smallest monomer member with the herringbone crystal structure, typical of acenes. Furthermore, there is a plethora of experimental vibrational spectra available for both gas and solid crystalline phases, allowing a detailed comparison between calculated and experimental values. The first extensive Raman and infrared (IR) studies of solid naphthalene were reported by Nedungadi [43] and Pimentel and McClellan [44]. Since then, numerous experiments have been performed to understand and assign the vibrational spectra [45–54], in particular that of Natkaniec *et al.* [49], who used coherent inelastic neutron scattering to map out phonon dispersion curves of deuterated naphthalene along several directions in the Brillouin zone.

Prior computational work on the phonon spectrum of solid naphthalene used semiempirical force-field methods, with parameters fit from experiments, for generation of both zone-center frequencies [55–59] and wave-vector-dependent dispersion [48,60–63], greatly aiding in the interpretation of

*altvater@berkeley.edu
†jbneaton@berkeley.edu

the naphthalene phonon spectra. More recently, the vibrational modes of gas-phase naphthalene—in particular, infrared and Raman active modes—as well as the zone-center modes of crystalline naphthalene have also been reproduced successfully with *ab initio* methods [53,59,64–68], although the mode assignments depend somewhat on the level of theory and functional [53,68]. Finally, Schatschneider *et al.* [69] and Reilly and Tkatchenko [70] used vdW-corrected DFT to obtain the zero-point energy and vibrational contribution (integrated over the Brillouin zone) to the lattice energy of several acenes, respectively, using the Tkatchenko-Scheffler pairwise approach; however, these studies did not provide any details of the phonon spectrum.

To our knowledge, only two *ab initio* phonon band structures of acene crystals have been reported to date [71,72]. The full phonon dispersion of tetracene was recently calculated using the local density approximation (LDA), capitalizing on the tendency of LDA to overbind to partially compensate for the lack of vdW corrections [72]. Band structures of solid naphthalene calculated at different pressures have been presented by Fedorov *et al.* [71] using the DFT-D3 approach [40] but without any detailed comparison with experiment. Considering the fundamental importance of phonons in organic crystals, there remains a need to assess and understand the efficacy of existing approaches for calculating phonon dispersions over the entire Brillouin zone in vdW-bound solids, particularly in the context of a well-characterized system such as naphthalene.

In this work, we compute the phonon dispersion of solid naphthalene within DFT using LDA, the generalized gradient approximation of Perdew, Burke, and Ernzerhof (PBE), and the recently developed nonlocal density functional vdW-DF-cx [73]. We provide the first detailed comparison between computed and measured phonon spectra of a molecular crystal across the Brillouin zone, assessing our results against neutron-scattering experiments on perdeuterated naphthalene, as well as IR and Raman spectra of solid perprotonated naphthalene. Our results show that vdW-DF-cx is able to reproduce both the ground-state structure and the full phonon dispersion with high accuracy. Lacking any long-range correlation, PBE overestimates the unit-cell volume by 29% percent and, as a result, significantly underestimates phonon frequencies relative to experiment. Notably, upon constraining the lattice parameters to experimental values, PBE yields good agreement, suggesting that it may reproduce phonon spectra for other organic crystals with known experimental geometry. LDA, in contrast, overbinds the naphthalene crystal as expected, resulting in a primitive cell volume that is 10% smaller than experiment and significantly overestimated phonon frequencies.

II. METHODS

For all calculations of solid naphthalene, we use density functional theory with a plane-wave basis and norm-conserving Troullier-Martins pseudopotentials [74], employing the software suite QUANTUM ESPRESSO version 5.1.1 [75]. We perform calculations with the LDA, PBE, and vdW-DF-cx (DF-cx) functionals. A kinetic energy cutoff of 110 Ry converges the total energy for all three functionals to
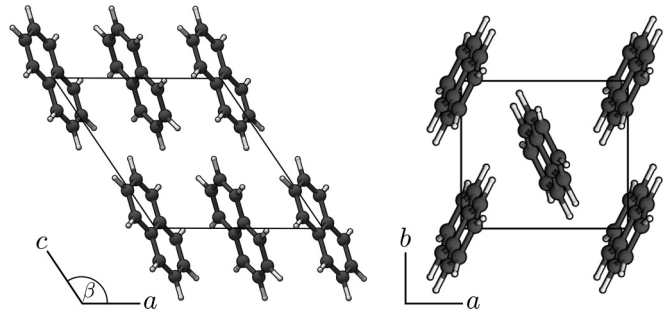

FIG. 1. Crystal structure of naphthalene. Naphthalene takes up a structure with the $P2_1/a$ space group, and with two molecules in the unit cell, each situated at inversion centers.

within 1 meV/atom. Calculations with DF-cx use the PBE pseudopotentials. As shown here and in our previous work [76], DF-cx is able to reproduce structural and electronic properties of acene crystals with high accuracy; e.g., lattice parameters are within 1% of experiment.

As starting geometry for all calculations, we use the experimental crystal structure of naphthalene measured at 5 K [77], available at the Cambridge Structural Database [78] (ID: NAPHTHA31). Naphthalene belongs to the $P2_1/a$ space group and contains two molecules per unit cell, each of which is situated at an inversion center. The molecules form a layered herringbone structure, with layers stacked in the c direction. The naphthalene unit cell is depicted in Fig. 1.

For relaxed lattice parameters we use the values obtained in our previous work [76], which converge the total energy to 1×10^{-5} Ry, using a Monkhorst-Pack **k**-grid of $8 \times 11 \times 8$. The calculated lattice parameters for all three functionals are given in Table I. Prior to the phonon calculations, all internal coordinates are relaxed again, while keeping the lattice parameters fixed and the symmetry constrained, using a smaller Monkhorst-Pack grid of $2 \times 4 \times 2$ (corresponding to the mesh used in our phonon calculations; see below). The Hellmann-Feynman forces are converged to 2×10^{-5} Ry/bohr and the total energy to 1×10^{-8} Ry. To ensure accurate forces, the convergence threshold for all self-consistent calculations is 1×10^{-12} Ry. We distinguish phonon dispersions obtained at experimental and relaxed lattice parameters by denoting results using experimental lattice parameters with "@Ω_{expt}," lattice parameters relaxed with LDA with "@Ω_{LDA}," etc.

Phonon band structures are calculated within a harmonic approximation via a finite-difference (FD) approach with a

TABLE I. Experimental and calculated lattice parameters for naphthalene [76]. Lattice constants a, b, and c are in angstroms, unit-cell volume Ω in $\mathring{A}^3$, and angle β in degrees.

	Expt. [78]	DF-cx	LDA	PBE
a	8.08	8.06	7.74	9.13
b	5.93	5.91	5.76	6.31
c	8.63	8.75	8.37	8.99
β	124.7	124.4	125.5	122.1
Ω	340.4	344.4	304.0	438.9

$2 \times 4 \times 2$ supercell, using Γ-point sampling. For zone-center phonon calculations, a single primitive cell with a centered Monkhorst-Pack **k**-grid of $2 \times 4 \times 2$ is used, commensurate with the supercell size above. We displace each atom by 0.00125 Å to generate the force constants in our FD approach. The frequency spectrum at each **q**-point is obtained by diagonalizing the Fourier transform of the real-space force-constant matrix. The acoustic sum rule is enforced. For LDA and PBE, our FD approach is in quantitative agreement with density functional perturbation theory. Mode numbering throughout this work includes the three acoustic modes; i.e., the first nonzero mode at Γ is designated as "mode 4." We use 1.00794 a.u. for the mass of the hydrogen atoms in perprotonated (d0) naphthalene or 2.01410 a.u. for those in perdeuterated (d8) naphthalene, depending on the hydrogen isotope present in the experiment we compare to. In plotting our phonon band structures, we follow Ref. [49] for our high-symmetry points and lines in **q**-space; however, the labels are adopted from the more contemporary Ref. [79]. As the experimental spectrum by Natkaniec *et al.* [49] was obtained at 6 K, we assume anharmonic effects are negligible, and our comparison with the FD method within the harmonic approximation is valid.

III. RESULTS AND DISCUSSION

We divide the discussion of our results into two parts. First, we discuss the intermolecular modes at lower frequency, comparing the performance of different density functionals to experiment. Then, we concentrate our analysis on the intramolecular modes at higher frequencies calculated with DF-cx and compare our results to IR and Raman measurements. In accord with prior work [49,59,71], we find that the phonon band structure shows a gap of roughly 40 cm^{-1} between the intermolecular and intramolecular modes. While we do confirm the observation of Coropceanu *et al.* [59] that all translational modes show slight internal bending motion, the mixing between inter- and intramolecular modes is very small and can be neglected for the purpose of classification.

A. Intermolecular modes

In Fig. 2 we show the phonon band structures of d8-naphthalene, in an energy window below 150 cm^{-1} focused on the intermolecular modes, calculated with the vdW nonlocal functional DF-cx, and with LDA and PBE. Given that PBE leads to a large overestimate of the lattice parameters, we only provide the phonon dispersion for PBE calculated by constraining the lattice parameters to those of experiment. The results are compared to experimental data obtained by neutron scattering of d8-naphthalene at 6 K [49].

At first glance, all three functionals reproduce the experimental curves quite well. The mean absolute percent deviation from experimental data points is 7.8% for DF-cx, 5.8% for PBE (at the experimental geometry), and 12.3% for LDA. These results are consistent with prior reports that PBE at experimental lattice parameters and LDA with relaxed parameters can yield good agreement for naphthalene (at the zone center) and tetracene (throughout the zone), respectively [59,72].

A major drawback of the PBE functional for naphthalene is that it requires prior knowledge of the experimental lattice parameters. If the naphthalene unit cell is optimized with PBE, the calculated volume is overestimated by 29% (Table I). Similar overestimates have been noted by Byrd *et al.* [80] for more polar molecular crystals. The calculated frequencies at this grossly overestimated volume decrease dramatically, as can be seen in Table II. Thus, using PBE to calculate phonon frequencies of organic crystals can only be efficacious for systems with known lattice parameters.

Despite being a purely local functional, LDA is known to lead to lattice parameters in agreement with experiment for certain vdW materials due to a cancellation of errors [81,82]. For naphthalene, the cancellation is apparently incomplete and the LDA optimized unit-cell volume is 10% smaller than experiment (Table I), a significant underestimate that leads, in turn, to an overestimate of the phonon frequencies. Thus, in general, the LDA is insufficient for quantitative prediction of phonon band structures of vdW-bound organic crystals. Interestingly, and unlike PBE, using experimental lattice parameters with LDA results in frequencies far below the experimental values (Table II). Evidently, the PBE gradient

TABLE II. Intermolecular mode frequencies of d8-naphthalene at Γ. Experimental values are taken from neutron-scattering experiments and compared to frequencies calculated with DF-cx, PBE, and LDA using experimental as well as relaxed lattice parameters (all values in cm^{-1}). Modes are ordered to best correspond to the symmetries reported experimentally.

| Mode | Symmetry (type) | Expt. [49] | DF-cx | | LDA | | PBE | |
			@$\Omega_{\text{DF-cx}}$	@Ω_{expt}	@Ω_{LDA}	@Ω_{expt}	@Ω_{PBE}	@Ω_{expt}
4	B_g (libr.)	54.37	50.20	54.27	58.69	23.90	18.88	46.26
5	A_u (trans.)	57.71	52.54	55.08	66.29	49.39	25.90	55.75
6	A_g (libr.)	64.38	59.03	68.08	73.02	43.74	21.09	54.68
7	B_u (trans.)	78.05	70.70	71.43	88.32	65.20	49.03	73.14
8	B_g (libr.)	79.39	74.19	80.64	88.58	54.90	43.04	77.25
9	A_g (libr.)	84.06	77.23	83.51	95.46	57.31	45.30	80.37
10	A_u (trans.)	106.74	97.42	99.33	118.65	75.32	47.78	107.39
11	A_g (libr.)	112.41	112.23	112.02	119.42	76.09	38.67	105.48
12	B_g (libr.)	130.09	128.83	130.55	141.33	94.93	48.72	124.98
Mean absolute deviation (cm^{-1})			4.83	2.37	9.52	27.18	51.28	4.41
Mean absolute percent deviation (%)			5.96	2.77	10.84	30.13	55.38	5.37
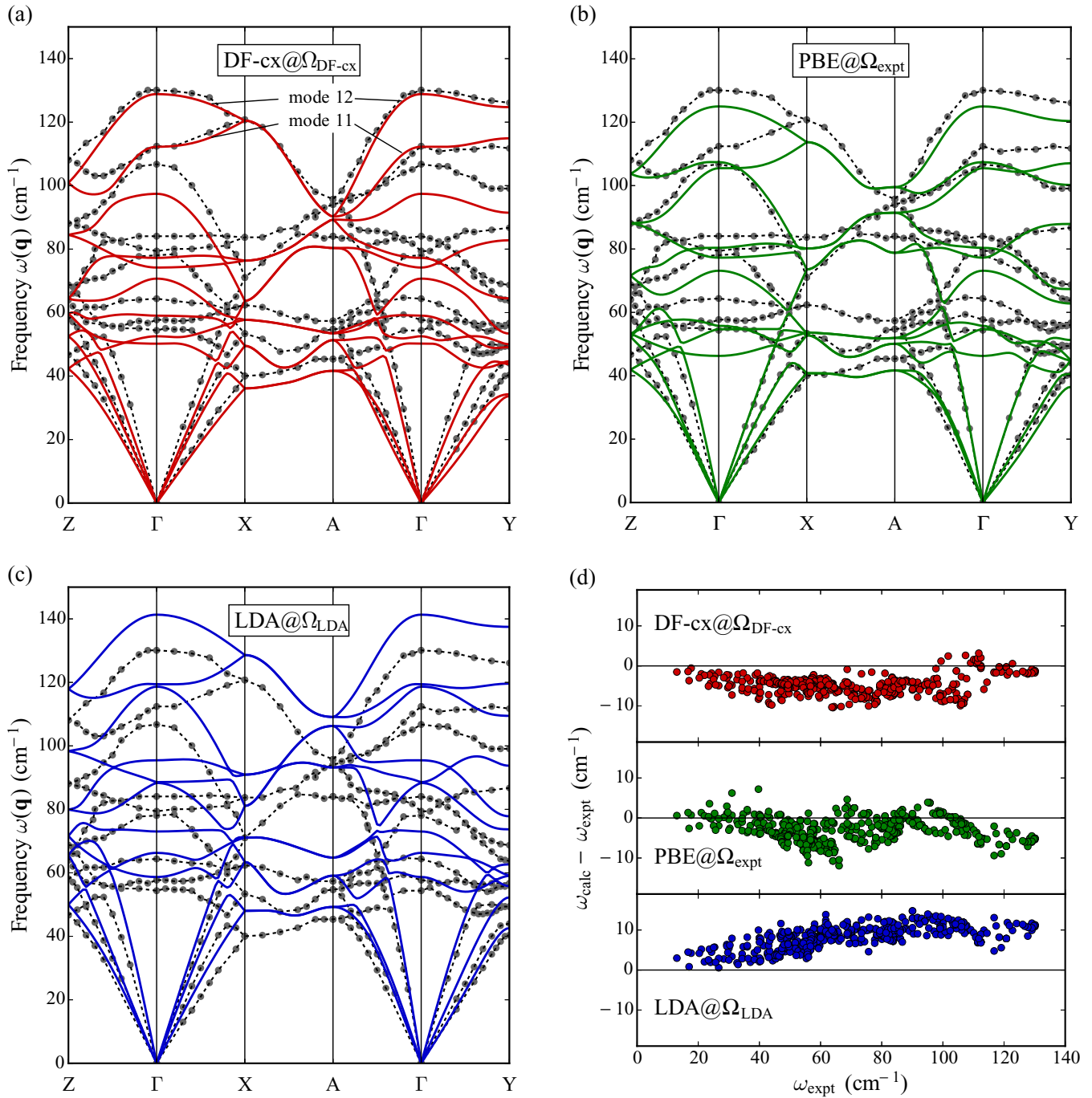
FIG. 2. Calculated phonon dispersion (solid lines), shown and analyzed in a frequency range dominated by intermolecular modes and compared with neutron-scattering experiments of d8-naphthalene at 6 K [49] (grey circles; dashed lines to guide the eye). While (a) DF-cx@$\Omega_{\text{DF-cx}}$ and (c) LDA@Ω_{LDA} use optimized lattice parameters, (b) PBE@Ω_{expt} results are shown as computed with experimental parameters. (d) The level agreement is quantified by plotting the difference between the calculated and the experimental values as a function of the latter. For the intermolecular modes DF-cx@$\Omega_{\text{DF-cx}}$ shows a mean absolute percent deviation of 7.8%, PBE@Ω_{expt} 5.8%, and LDA@Ω_{LDA} 12.3%.

corrections restore repulsive short-range intermolecular interactions missing in LDA, leading to agreement with experiment at the experimental lattice parameters.

DF-cx, on the other hand, predicts the naphthalene unit-cell volume within 1% [76] while reproducing the experimental intermolecular frequencies within 7.8%. Although the total deviation is slightly larger than for PBE, the scatter plot in Fig. 2 shows that the DF-cx frequencies below 100 cm^{-1} are

shifted by a more or less constant factor, while PBE errors are more randomly distributed over the range of intermolecular modes, indicating that DF-cx better reproduces the qualitative structure of the phonon dispersion. The superior performance of DF-cx for phonons is further evident when comparing the calculated bandwidths of the two lowest optical bands. While PBE and LDA display a pronounced minimum and maximum for the first and second optical bands centered on Γ along
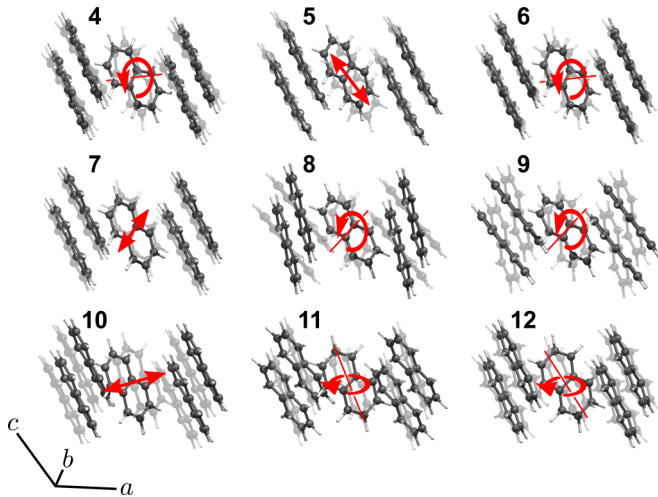
FIG. 3. The nine intermolecular optical modes of crystalline naphthalene. Modes 5, 7, and 10 are translational modes roughly parallel to *c*, *b*, and *a*, respectively. The other modes are librational modes with rotational axes roughly along *a* (4, 6), *b* (8, 9), and *c* (11, 12).

$Z \rightarrow \Gamma \rightarrow X$, DF-cx reproduces the saddle-point-like dispersion reported in experiment. Additionally, along the high-symmetry line $X \rightarrow A$, the slope of the lowest band calculated with DF-cx matches the experimental spectrum, whereas both PBE and LDA, incorrectly, predict a minimum. Clearly these soft intermolecular modes, where the influence of nonlocal vdW dispersive forces would be expected to be most significant, have the largest dependence on the chosen functional, and LDA and PBE exhibit the largest discrepancies. Overall, DF-cx, which accounts for vdW-dispersion forces, is more predictive and performs significantly better than either PBE or LDA for these low-lying naphthalene intermolecular modes across the Brillouin zone.

We now comment further on the systematic underestimation of the frequencies of the first ten bands for DF-cx. If this were simply due to an overall underestimate of intermolecular forces, we would expect all frequencies to be uniformly redshifted. However, the two highest bands (modes 11 and 12) along $\Gamma \rightarrow X$ and along $\Gamma \rightarrow Y$ show excellent agreement (see Fig. 2). What distinguishes these two modes from the others? These are librational modes with the libration axes roughly along the length of the molecules and parallel to the *c* axis. (See Fig. 3 for a visualization of the displacement vectors at Γ.) The nature of the libration in modes 11 and 12 is such that the atom-atom distances between molecular layers remain relatively constant compared to the other modes. The two modes are thus dominated by interactions within the *ab* plane. Now, if we inspect the lattice parameters in Table I more closely, we see that the 1% volume difference is mainly caused by an elongated *c* axis, while *a* and *b* are much closer to experimental values. The longer *c* axis results in weaker interactions along that direction and overall lower frequencies for displacements with the largest amplitudes between layers, explaining the different behavior of modes 11 and 12 (which have minimal amplitude along *c*) compared to the rest.

Further support for this explanation can be found at the high-symmetry points Z and A, where DF-cx underestimates

the frequencies of the two highest intermolecular mode bands relative to experiment. The coupling of those two modes at Z leads to a shift of the rotational axes to the edge of the molecule. The displacement pattern associated with these modes could be described as a flapping motion, similar to a flag on a pole in the wind, and leads to atomic displacements much further into the interlayer gap (and heightened sensitivity to *c*). In contrast, at X, the rotational axes remain centered on the molecules, and these calculated frequencies exhibit the same excellent agreement with experiment as observed at Γ. Finally, at the high-symmetry point A, we observe near degeneracy between the four modes 9–12. The mixing between the two librational modes 11 and 12 with the translational mode 10 along *a*, and a librational mode with rotation axes along *b*, again leads to mode displacement patterns with higher amplitudes between molecular layers and an underestimate relative to experiment. In sum, we can associate the underestimation of frequencies of many of the intermolecular modes by DF-cx directly to the overestimate of the *c*-axis parameter relative to experiment.

We can quantify this analysis further by comparing the frequencies calculated with experimental lattice parameters (DF-cx@Ω_{expt}) to the corresponding frequencies of DF-cx@Ω_{DF-cx}. Indeed, most zone-center frequencies are shifted upwards to give much better agreement with experiment, as can also be seen by the much improved mean average and percent deviation (Table II). The mode frequencies are notably sensitive to a small change in lattice parameters, essentially 1% along one axis. For example, in the case of mode 6 we compute an increase of 15%, and an overall decrease in the mean percent deviation by more than a factor of 2.

We note that the frequencies of modes 7 and 10, translational modes along the *b* and *a* axes, respectively, are largely unaffected by the change in lattice parameters and continue to deviate from experiment in both cases by 7–10%. This remaining disagreement with experiment may at least partially be associated with limitations of DF-cx. In addition, there are still uncertainties regarding experimental and calculated lattice parameters. The crystals used in the neutron-diffraction experiments (d8-naphthalene) might exhibit small differences from the d0-naphthalene structure measured by Capelli *et al.* [77], which we use in this work. In fact, d8-naphthalene is known to exhibit small quantitative differences in lattice parameters relative to its perprotonated counterpart, resulting in a difference in volume of about 0.5% at room temperature [83,84]. As this volume difference might be a finite-temperature effect, its implications are not directly transferable to our low-temperature study, however. On the other hand, our calculated relaxed lattice parameters do not take into account finite-temperature effects or zero-point anharmonic expansion, which could increase the calculated cell volume even at 0 K [85–87]. Considering the impact on the phonon dispersion caused by the ~ 1% change in volume, as shown above, such small differences in cell volume could account for the remaining discrepancies between DF-cx and experiment.

In conclusion, accurate determination of lattice parameters is central for the *ab initio* calculation of intermolecular phonon frequencies in vdW-bound crystals. As we have shown, DF-cx outperforms the conventional functionals LDA and PBE and is able to reproduce qualitatively and quantitatively the

dispersion of intermolecular modes across the Brillouin zone of solid naphthalene.

B. Intramolecular modes

We now turn our discussion to the intramolecular modes above $150\,\mathrm{cm}^{-1}$. Relaxations with the three functionals used here lead to very similar internal coordinates, within 0.015 Å, or 1% for bond lengths and 0.3°, or 0.2% for angles (see Table S1 in the Supplemental Material (SM) [88] for all relaxed coordinates). As a result, all functionals predict very similar frequencies for intramolecular modes, agreeing to within 2.5% (Table S2 and Fig. S1 in the SM [88]); in contrast, intermolecular frequencies (discussed above) differ from DF-cx by 6.3–25% for LDA, and 2.9–10% for PBE. Thus, in what follows, we limit ourselves to the analysis of DF-cx results. In order to compare with experiments on d0-naphthalene, we present both deuterated and nondeuterated naphthalene results. Figure 4 shows both full isotopic band structures side by side for comparison. To illustrate the isotope shifts of individual zone center modes, we connect the frequencies corresponding to the two eigenvectors with the largest projection with black lines. For all frequencies and corresponding shifts see Table S3 in the SM [88].

Interestingly, hydrogenation leads to isotope shifts $\omega_\mathrm{H}/\omega_\mathrm{D}$ with a rather large spread, from 0.998 to 1.394, and results in considerable reordering of the normal modes. Notably, for the two C-C stretch modes at around $1390\,\mathrm{cm}^{-1}$, we predict a rather unexpected decrease in frequency by about $3\,\mathrm{cm}^{-1}$ for d0- compared to d8-naphthalene. This can be explained by additional strain on the bond angles, as the more inert deuterium atoms do not displace as much with the carbon atoms. The modified displacement pattern leads to an effective increase in the force constant which more than negates the effect of the higher mass. Additionally, the almost constant shift of 1.35 for all high-frequency C-H stretch modes at around $2275\,\mathrm{cm}^{-1}$ and $3075\,\mathrm{cm}^{-1}$, respectively, corresponds almost exactly to the expected shift of $\sqrt{m_\mathrm{D}/m_\mathrm{H}} = 1.36$.

Finally, we compare calculated DF-cx zone-center frequencies of d0-naphthalene with experimental IR and Raman frequencies measured and reported by Suzuki *et al.* [46]. (All frequencies are listed in Table S2 in the SM [88]. For visual comparison, we indicate the experimental values with black circles along the Γ point in the spectrum in Fig. 4.) Overall, the agreement between theory and experiment is excellent, resulting in a mean absolute deviation of 1%. Discrepancies between experimental and calculated values can have several origins. The IR and Raman measurements were performed at room temperature, which lead to increased anharmonic contributions, generally lowering the measured frequencies relative to those computed within a harmonic approximation. Another complication is the assignment of experimental frequencies. Overtones and combination bands in a dense spectrum may be challenging to distinguish from fundamental frequencies. This can obfuscate mode assignments, as can be nicely seen in the large table assembled by Lielmezs *et al.* [51]. To help with the future comparison with these data, we list all calculated frequencies and their respective symmetries in the SM [88].
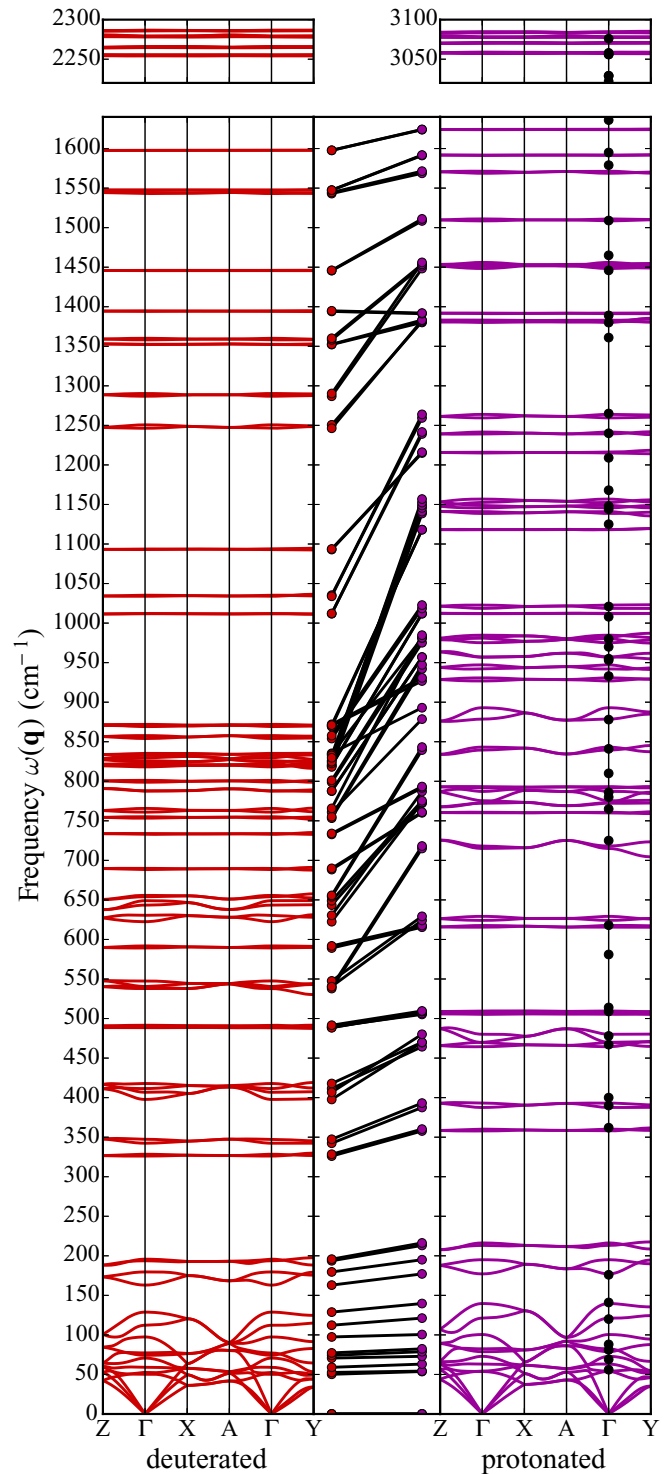

FIG. 4. Comparison between phonon dispersion curves calculated with DF-cx of d8- and d0-naphthalene. The black lines in the center illustrate the shift of zone-center frequencies (dots) by connecting the two modes with the highest projection between eigenvectors. The black circles along Γ in the perprotonated spectrum on the right are experimental IR and Raman frequencies of solid naphthalene [46]. The intermolecular frequencies below $150\,\mathrm{cm}^{-1}$ were measured at 4 K, the intramolecular frequencies at room temperature. For the distinction between IR and Raman active modes, see Table S2 in the Supplemental Material [88].

IV. CONCLUSION

In this work, we calculated the full phonon dispersion of d8- and d0-naphthalene with density functional theory. We evaluated results obtained with three different density functionals, namely LDA, PBE, and vdW-DF-cx. Comparing the resulting dispersion of the intermolecular modes to the experimental data obtained with neutron scattering, we highlighted the necessity of using a vdW-corrected approach to accurately predict the phonon spectrum. More specifically, we find that PBE fails to predict bulk lattice parameters for naphthalene that result in reasonable frequencies relative to experiment. However, using experimental lattice parameters, PBE can lead to relatively accurate phonon dispersion (although qualitative discrepancies remain for intermolecular modes). LDA underestimates the unit cell by 10% and consistently overestimates the frequencies; unlike PBE, LDA performs significantly worse at experimental lattice parameters. DF-cx, on the other hand, captures both the ground-state geometry of the crystal as well as the phonon dispersion, both quantitatively and qualitatively. The small discrepancies with respect to experiment are likely due to modest differences between the predicted lattice parameters and experiments, as well as any differences between the experimental structures of d0- and d8-naphthalene.

Further, we presented calculations of the full phonon dispersion of both d8- and d0-naphthalene, and compared the Γ-point frequencies of d0-naphthalene to experimental values obtained by IR and Raman spectroscopy. Being less sensitive to long-range intermolecular interactions and lattice parameters, excellent agreement with intramolecular mode frequencies was obtained by all three functionals.

This study demonstrates that including vdW interactions in the functional is crucial in order to obtain predictive structural and vibrational properties for weakly bound organic crystals and related materials like naphthalene. DF-cx, while already performing well, is only one of many existing and potential vdW approaches, and crystalline naphthalene is one of the simplest organic crystals. Our study provides further insight into the vibrational properties of these materials across the Brillouin zone and is a starting point for benchmarking other vdW methods with naphthalene and known molecular crystals.

[1] D. R. Gamota, P. Brazis, K. Kalyanasundaram, and J. Zhang, *Printed Organic and Molecular Electronics*, edited by D. Gamota, P. Brazis, K. Kalyanasundaram, and J. Zhang (Springer, Boston, 2004).

[2] S. Mandal and Y.-Y. Noh, Semicond. Sci. Technol. **30**, 064003 (2015).

[3] S.-Y. Min, T.-S. Kim, Y. Lee, H. Cho, W. Xu, and T.-W. Lee, Small **11**, 45 (2015).

[4] E. Menard, V. Podzorov, S.-H. Hur, A. Gaur, M. E. Gershenson, and J. A. Rogers, Adv. Mater. **16**, 2097 (2004).

[5] J. Takeya, M. Yamagishi, Y. Tominari, R. Hirahara, Y. Nakazawa, T. Nishikawa, T. Kawase, T. Shimoda, and S. Ogawa, Appl. Phys. Lett. **90**, 102120 (2007).

[6] J. E. Anthony, Chem. Rev. **106**, 5028 (2006).

[7] J. E. Anthony, Angew. Chemie Int. Ed. **47**, 452 (2008).

[8] G. Schweicher, Y. Olivier, V. Lemaur, and Y. H. Geerts, Isr. J. Chem. **54**, 595 (2014).

[9] M. B. Smith and J. Michl, Chem. Rev. **110**, 6891 (2010).

[10] M. B. Smith and J. Michl, Annu. Rev. Phys. Chem. **64**, 361 (2013).

[11] X.-Y. Zhu, Q. Yang, and M. Muntwiler, Acc. Chem. Res. **42**, 1779 (2009).

[12] D. N. Congreve, J. Lee, N. J. Thompson, E. Hontz, S. R. Yost, P. D. Reusswig, M. E. Bahlke, S. Reineke, T. Van Voorhis, and M. A. Baldo, Science **340**, 334 (2013).

[13] J. Lee, P. Jadhav, P. D. Reusswig, S. R. Yost, N. J. Thompson, D. N. Congreve, E. Hontz, T. Van Voorhis, and M. A. Baldo, Acc. Chem. Res. **46**, 1300 (2013).

[14] W.-L. Chan, T. C. Berkelbach, M. R. Provorse, N. R. Monahan, J. R. Tritsch, M. S. Hybertsen, D. R. Reichman, J. Gao, and X.-Y. Zhu, Acc. Chem. Res. **46**, 1321 (2013).

[15] J.-L. Brédas, J. E. Norton, J. Cornil, and V. Coropceanu, Acc. Chem. Res. **42**, 1691 (2009).

[16] F. Ortmann, F. Bechstedt, and K. Hannewald, Phys. Status Solidi **248**, 511 (2011).

[17] M. L. Tiago, J. E. Northrup, and S. G. Louie, Phys. Rev. B **67**, 115212 (2003).

[18] K. Hummer, P. Puschnig, and C. Ambrosch-Draxl, Phys. Rev. B **67**, 184105 (2003).

[19] K. Hummer, P. Puschnig, and C. Ambrosch-Draxl, Phys. Rev. Lett. **92**, 147402 (2004).

[20] K. Hummer and C. Ambrosch-Draxl, Phys. Rev. B **72**, 205205 (2005).

[21] J. B. Neaton, M. S. Hybertsen, and S. G. Louie, Phys. Rev. Lett. **97**, 216405 (2006).

[22] C. Ambrosch-Draxl, D. Nabok, P. Puschnig, and C. Meisenbichler, New J. Phys. **11**, 125010 (2009).

[23] S. Sharifzadeh, A. Biller, L. Kronik, and J. B. Neaton, Phys. Rev. B **85**, 125307 (2012).

[24] P. Cudazzo, M. Gatti, and A. Rubio, Phys. Rev. B **86**, 195307 (2012).

[25] P. Cudazzo, M. Gatti, A. Rubio, and F. Sottile, Phys. Rev. B **88**, 195152 (2013).

[26] P. Cudazzo, F. Sottile, A. Rubio, and M. Gatti, J. Phys. Condens. Matter **27**, 113204 (2015).

[27] S. Refaely-Abramson, S. Sharifzadeh, M. Jain, R. Baer, J. B. Neaton, and L. Kronik, Phys. Rev. B **88**, 081204 (2013).

[28] S. Refaely-Abramson, M. Jain, S. Sharifzadeh, J. B. Neaton, and L. Kronik, Phys. Rev. B **92**, 081204 (2015).

[29] D. Nabok, P. Puschnig, and C. Ambrosch-Draxl, Phys. Rev. B **77**, 245316 (2008).

[30] L. Kronik and A. Tkatchenko, Acc. Chem. Res. **47**, 3208 (2014).

[31] M. Dion, H. Rydberg, E. Schröder, D. C. Langreth, and B. I. Lundqvist, Phys. Rev. Lett. **92**, 246401 (2004).

[32] K. Lee, É. D. Murray, L. Kong, B. I. Lundqvist, and D. C. Langreth, Phys. Rev. B **82**, 081101 (2010).

[33] K. Berland, V. R. Cooper, K. Lee, E. Schröder, T. Thonhauser, P. Hyldgaard, and B. I. Lundqvist, Rep. Prog. Phys. **78**, 066501 (2015).

[34] A. Tkatchenko and M. Scheffler, Phys. Rev. Lett. **102**, 073005 (2009).

[35] R. A. DiStasio, O. A. von Lilienfeld, and A. Tkatchenko, Proc. Natl. Acad. Sci. USA **109**, 14791 (2012).

[36] W. Liu, V. G. Ruiz, G.-X. Zhang, B. Santra, X. Ren, M. Scheffler, and A. Tkatchenko, New J. Phys. **15**, 053046 (2013).

[37] N. Ferri, R. A. DiStasio, A. Ambrosetti, R. Car, and A. Tkatchenko, Phys. Rev. Lett. **114**, 176802 (2015).

[38] S. Grimme, J. Comput. Chem. **25**, 1463 (2004).

[39] S. Grimme, J. Comput. Chem. **27**, 1787 (2006).

[40] S. Grimme, J. Antony, S. Ehrlich, and H. Krieg, J. Chem. Phys. **132**, 154104 (2010).

[41] P. L. Silvestrelli, Phys. Rev. Lett. **100**, 053002 (2008).

[42] P. L. Silvestrelli, K. Benyahia, S. Grubisiĉ, F. Ancilotto, and F. Toigo, J. Chem. Phys. **130**, 074702 (2009).

[43] T. M. K. Nedungadi, Proc. Indian Acad. Sci. Sect. A **15**, 376 (1942).

[44] G. C. Pimentel and A. L. McClellan, J. Chem. Phys. **20**, 270 (1952).

[45] J. Hollas, J. Mol. Spectrosc. **9**, 138 (1962).

[46] M. Suzuki, T. Yokoyama, and M. Ito, Spectrochim. Acta A **24**, 1091 (1968).

[47] D. M. Hanson, J. Chem. Phys. **51**, 5063 (1969).

[48] G. A. Mackenzie, G. S. Pawley, and O. W. Dietrich, J. Phys. C Solid State Phys. **10**, 3723 (1977).

[49] I. Natkaniec, E. L. Bokhenkov, B. Dorner, J. Kalus, G. A. Mackenzie, G. S. Pawley, U. Schmelzer, and E. F. Sheka, J. Phys. C Solid State Phys. **13**, 4265 (1980).

[50] E. L. Bokhenkov, A. I. Kolesnikov, T. A. Krivenko, E. F. Sheka, V. A. Dementjev, and I. Natkaniec, J. Phys. Colloq. **42**, C6-605 (1981).

[51] J. Lielmezs, F. Bennett, and D. McFee, Thermochim. Acta **47**, 287 (1981).

[52] E. F. Sheka, E. L. Bokhenkov, B. Dorner, J. Kalus, G. A. Mackenzie, I. Natkaniec, G. S. Pawley, and U. Schmelzer, J. Phys. C Solid State Phys. **17**, 5893 (1984).

[53] A. Srivastava and V. B. Singh, Indian J. Pure Appl. Phys. **45**, 714 (2007).

[54] K. P. Meletov, Phys. Solid State **55**, 581 (2013).

[55] E. Huler and A. Warshel, Chem. Phys. **8**, 239 (1975).

[56] V. K. Jindal and J. Kalus, J. Phys. C Solid State Phys. **16**, 3061 (1983).

[57] R. G. Della Valle, E. Venuti, and A. Brillante, Chem. Phys. **198**, 79 (1995).

[58] G. M. Day, S. L. Price, and M. Leslie, J. Phys. Chem. B **107**, 10919 (2003).

[59] V. Coropceanu, R. S. Sánchez-Carrera, P. Paramonov, G. M. Day, and J. L. Brédas, J. Phys. Chem. C **113**, 4679 (2009).

[60] G. S. Pawley, Phys. Status Solidi **20**, 347 (1967).

[61] G. S. Pawley and S. J. Cyvin, J. Chem. Phys. **52**, 4073 (1970).

[62] R. Righini, S. Califano, and S. Walmsley, Chem. Phys. **50**, 113 (1980).

[63] V. Schettino and S. Califano, J. Mol. Struct. **100**, 459 (1983).

[64] N. Rougeau, J. Flament, P. Youkharibache, H. Gervais, and G. Berthier, J. Mol. Struct. THEOCHEM **254**, 405 (1992).

[65] F. Pauzat, D. Talbi, M. D. Miller, D. J. DeFrees, and Y. Ellinger, J. Phys. Chem. **96**, 7882 (1992).

[66] E. Cebe and G. Grampp, Z. Phys. Chem. **187**, 15 (1994).

[67] S. R. Langhoff, J. Phys. Chem. **100**, 2819 (1996).

[68] C. W. Bauschlicher and S. R. Langhoff, Spectrochim. Acta A **53**, 1225 (1997).

[69] B. Schatschneider, J. J. Liang, A. M. Reilly, N. Marom, G. X. Zhang, and A. Tkatchenko, Phys. Rev. B **87**, 060104 (2013).

[70] A. M. Reilly and A. Tkatchenko, J. Chem. Phys. **139**, 024705 (2013).

[71] I. Fedorov, F. Marsusi, T. Fedorova, and Y. Zhuravlev, J. Phys. Chem. Solids **83**, 24 (2015).

[72] M. Abdulla, K. Refson, R. H. Friend, and P. D. Haynes, J. Phys. Condens. Matter **27**, 375402 (2015).

[73] K. Berland and P. Hyldgaard, Phys. Rev. B **89**, 035412 (2014).

[74] M. Fuchs and M. Scheffler, Comput. Phys. Commun. **119**, 67 (1999).

[75] P. Giannozzi, S. Baroni, N. Bonini, M. Calandra, R. Car, C. Cavazzoni, D. Ceresoli, G. L. Chiarotti, M. Cococcioni, I. Dabo, A. Dal Corso, S. de Gironcoli, S. Fabris, G. Fratesi, R. Gebauer, U. Gerstmann, C. Gougoussis, A. Kokalj, M. Lazzeri, L. Martin-Samos, N. Marzari, F. Mauri, R. Mazzarello, S. Paolini, A. Pasquarello, L. Paulatto, C. Sbraccia, S. Scandolo, G. Sclauzero, A. P. Seitsonen, A. Smogunov, P. Umari, and R. M. Wentzcovitch, J. Phys. Condens. Matter **21**, 395502 (2009).

[76] T. Rangel, K. Berland, S. Sharifzadeh, F. Brown-Altvater, K. Lee, P. Hyldgaard, L. Kronik, and J. B. Neaton, Phys. Rev. B **93**, 115206 (2016).

[77] S. C. Capelli, A. Albinati, S. a. Mason, and B. T. M. Willis, J. Phys. Chem. A **110**, 11695 (2006).

[78] I. R. Thomas, I. J. Bruno, J. C. Cole, C. F. Macrae, E. Pidcock, and P. A. Wood, J. Appl. Crystallogr. **43**, 362 (2010).

[79] W. Setyawan and S. Curtarolo, Comput. Mater. Sci. **49**, 299 (2010).

[80] E. F. C. Byrd, G. E. Scuseria, and C. F. Chabalowski, J. Phys. Chem. B **108**, 13100 (2004).

[81] É. D. Murray, K. Lee, and D. C. Langreth, J. Chem. Theory Comput. **5**, 2754 (2009).

[82] K. Berland and P. Hyldgaard, Phys. Rev. B **87**, 205421 (2013).

[83] D. W. J. Cruickshank, Acta Crystallogr. **10**, 504 (1957).

[84] G. S. Pawley and E. A. Yeats, Acta Crystallogr. **B25**, 2009 (1969).

[85] A. Warshel, J. Chem. Phys. **53**, 582 (1970).

[86] B. P. van Eijck, J. Comput. Chem. **22**, 816 (2001).

[87] P. Hao, Y. Fang, J. Sun, G. I. Csonka, P. H. T. Philipsen, and J. P. Perdew, Phys. Rev. B **85**, 014111 (2012).

[88] See Supplemental Material at http://link.aps.org/supplemental/10.1103/PhysRevB.93.195206 for relaxed internal coordinates, a list of calculated frequencies compared to experimental IR and Raman spectra, the full band structures for all three functionals, as well as a complete list of isotope shift factors for DF-cx.